JOURNAL OF COMPUTATIONAL PHYSICS 104, 41–49 (1993)

A Suitable Boundary Condition for Bounded Plasma Simulation without Sheath Resolution

S. E. PARKER,* R. J. PROCASSINI,† AND C. K. BIRDSALL

Electronics Research Laboratory, University of California, Berkeley, California 94720

AND

B. I. COHEN

Magnetic Fusion Energy Division, Lawrence Livermore National Laboratory, Livermore, California 94550

Received February 26, 1990; revised May 7, 1991

We have developed a technique that allows for a sheath boundary layer *without* having to resolve the inherently small space and time scales of the sheath region. We refer to this technique as the *logical sheath* boundary condition. This boundary condition, when incorporated into a direct-implicit particle code, permits large space- and time-scale simulations of bounded systems, which would otherwise be impractical on current supercomputers. The lack of resolution of the collector sheath potential drop obtained from conventional implicit simulations at moderate values of $\omega_{pe}\Delta t$ and $\Delta z/\lambda_{De}$ provides the motivation for the development of the logical sheath boundary condition. The algorithm for use of the logical sheath boundary condition in a particle simulation is presented. Results from simulations which use the logical sheath boundary condition are shown to compare reasonably well with those from an analytic theory and simulations in which the sheath is resolved.

1. INTRODUCTION

The study of plasma flow from the bulk through the sheath region to an absorbing wall has a wide variety of applications. Virtually all experimental plasma devices have a wall, with an adjacent boundary layer, to which there is plasma transport. Here, we focus on unmagnetized systems or magnetized systems in which the flow of plasma is parallel to the magnetic field. Examples of this type of problem range from the simplest plasma discharges to relatively large and complex tokamak fusion experiments.

In the latter case, there is interest in understanding the flow of plasma through the scrape-off layer to the plates of a diverted tokamak [1–4]. The energy with which ions strike the divertor plate determines the physics of particle recycling and sputtering from the plate. Since the ion impact energy is significantly affected by the collector sheath potential drop in front of the plate, it is important to have an accurate prediction of the magnitude of this quantity. Previous particle simulations used for modeling plasma flow to a floating wall have fully resolved the sheath region [3–5]. Because the sheath is an inerently small space-scale ($\sim\lambda_{De}$) and time-scale ($\sim\omega_{pe}^{-1}$) structure (where ω_{pe} is the electron plasma frequency and λ_{De} is the electron Debye length), the numerical quantities $\omega_{pe}\Delta t$ and $\Delta z/\lambda_{De}$ (where Δt is the time step and Δz is the grid spacing) must be small for accurate resolution of the sheath region. These restrictions on the time step and grid cell size usually limit these simulations to artificially small mass ratios and/or short system lengths.

The development of implicit particle-in-cell (PIC) methods has eliminated the stability constraint on the size of the time step in time-explicit particle simulations [6–10]. This allows for the simulation of long-wavelength, low-frequency physics with coarse-grained temporal and spatial resolution (i.e., $\omega_{pe}\Delta t > 1$ and $\Delta z/\lambda_{De} > 1$), while damping out the unwanted high-frequency effects [11]. However, as we will show in this paper, the conventional direct-implicit PIC method does not accurately resolve short-range spatial effects (such as those found in the collector sheath region) when $\omega_{pe}\Delta t$ is large. Hence, we propose an alternative scheme which does *not* resolve the sheath region, yet provides an accurate description of the sheath potential drop and kinetic physics near the wall. We call this scheme the *logical sheath* boundary condition. This boundary condition maintains zero net current to the wall at each time step by absorbing all of the incident ions and an equal number of the fastest incident electrons. The slower electrons are reflected from the wall boundary. The collector

* Present Address: Princeton Plasma Physics Laboratory, P.O. Box 451, Princeton, NJ 08543

† Present Address: Lawrence Livermore National Laboratory, P.O. Box 808, Livermore, CA 94550

0021-9991/93 $5.00

sheath potential drop is determined from the incident velocity of the slowest absorbed electron. Hence, the overall sheath physics is retained and the small space- and time-scale resolution of the sheath region is not necessary.

This paper is organized in the following manner. The PIC models of the plasma-sheath region used for this study are described in Section 2. Section 3 presents the electrostatic potential profiles for these systems which are obtained from a conventional, direct-implicit particle code at small to moderate values of $\omega_{pe}\,\Delta t$ and $\Delta z/\lambda_{De}$. These results illustrate the inaccuracies associated with using $\omega_{pe}\,\Delta t \gtrsim \Delta z/\lambda_{De} \gtrsim 1$ to model sheath physics. The algorithm for incorporating the logical sheath boundary condition into a particle simulation code is discussed in Section 4. The logical sheath boundary condition is then used in a direct-implitic PIC code to calculate the collector sheath potential drop in the plasma-sheath models. The results from these simulations, which are presented in Section 5, are in agreement with those from an analytic theory and from conventional simulations in which the collector sheath region is fully resolved.

2. DESCRIPTION OF THE PLASMA-SHEATH MODEL

The one-dimensional models which are used in the study the flow of plasma from the bulk region through the sheath region to a floating, absorbing wall are shown schematically in Fig. 1. In each model, fully ionized, collisionless plasma fills the system over the range $0 \leqslant z \leqslant L$. The models are also assumed to be unmagnetized and electrostatic. A collector sheath potential drop forms over the first few electron Debye lengths to the left of the absorbing wall, which constitutes the right boundary of each system. The potential at this boundary floats at a potential ϕ_w, since the charge of all the particles that are absorbed is added to the surface of the wall (i.e., the wall is not grounded or connected to an external circuit). The electric field at the right boundary is proportional to the charge that has accumulated on the surface of the wall. The potential at the left boundary is fixed at zero. Particle and energy losses to the absorbing wall are balanced by the injection of plasma into the system from (i) a distributed source region ($0 \leqslant z \leqslant L_S \simeq 0.4L$; shown in Fig. 1a), or (ii) a planar source located at the left boundary ($z = 0$; shown in Fig. 1b). In the source-free region of each model, the potential is constant except for time-dependent fluctuations [1]. The unique features of each of these models will now be discussed separately.

2.1. *The Distributed Source Model*

The source region potential drop which forms within the distributed source region is a gradual potential variation, with a scale length equal to the width of the source region L_S. This potential drop develops in order to equilibrate the fluxes of electrons and ions that leave the source region, since the thermal velocity of the source electrons is, in general, greater than that of the source ions. Equal numbers of ions and electrons per unit length per time step are injected into the source region with velocities chosen from the source distribution function $S_s(z, v)$, which has a characteristic temperature kT_{s0}, for particles of species s. (For the balance of this paper, the subscript 0 shall designate source quantities.) The collector sheath and central regions are assumed to be source-free.

The left boundary of the system is a symmetry plane, such that the electric field at that location is zero, since no charge is accumulated there. The rethermalization or *refluxing* plane [3, 4], which is co-located with the symmetry plane at $z = 0$, simulates a large virtual region in which Coulomb collisions repopulate the tail of the electron distribution. The electrons in the tail of the distribution were energetic enough to overcome the collector sheath potential barrier

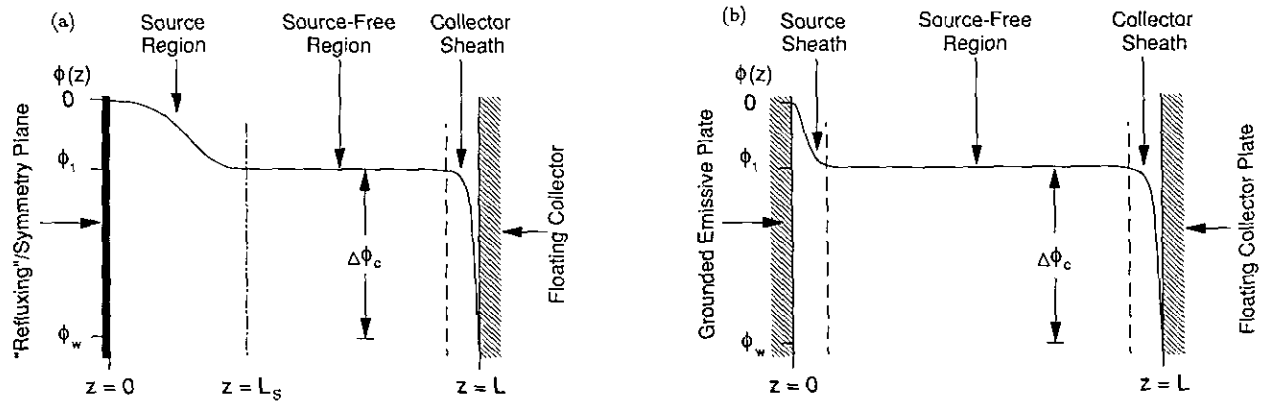

FIG. 1. A schematic diagram of the plasma-sheath models showing the absorbing wall and a characteristic potential profile: (a) the distributed source model and (b) the planar source model.

and be absorbed at the wall. As particles cross $z=0$ from right to left, their direction of travel is reversed and their speed is replaced by a value which is chosen from an *untruncated* half-Maxwellian with a thermal spread determined from the source temperature kT_{s0}. The refluxing process is the mechanism which allows the simulation to evolve to an equilibrium potential profile, even though the system is considered to be collisionless [4]. This is the only aspect of the particle simulation model which is *not* self-consistent. This model may be used to simulate plasma transport in the scrape-off layer of a diverted tokamak fusion device.

2.2. *The Planar Source Model*

The planar source model consists of an emissive wall (cathode) at $z=0$ which injects a flux of electrons and ions (Γ_e and Γ_i) towards the right and a fully absorbing wall (anode) at $z=L$. The cathode will also absorb any reentrant particles. A source region potential drop may form over a few Debye lengths adjacent to the cathode, depending upon the values of the injected flux ratio Γ_e/Γ_i and the injected-particle thermal velocity ratio v_{te0}/v_{ti0}. The balance of the system is assumed to be source free and collisionless. This model is applicable to the study of plasma discharges in a single-ended Q machine.

3. MOTIVATION FOR A SHEATH BOUNDARY CONDITION

This section presents the results of simulations which illustrate that an implicit PIC code's ability to accurately resolve the collector sheath region degrades as Δt is increased. This has been previously studied in Ref. [14]. This behavior motivates the replacement of the sheath region in the simulation with an alternate boundary condition that mimics the sheath physics. The one-dimensional, direct-implicit PIC code DIPSI [12] has been used to calculate the electrostatic potential structure in the collisionless plasma-sheath systems described in the previous section. DIPSI employs a variable-damping formulation of the direct-implicit equations of motion [13] and uses consistent boundary conditions for the direct-implicit method for the case of plasma in contact with a conducting, absorbing wall [14].

For each plasma-sheath system, a series of five simulations were performed in which the time steps and grid spacings were varied to cover the range from the explicit limit ($\Delta t \ll \omega_{pe}$ and $\Delta z < \lambda_{De}$) to the implicit limit ($\Delta t > \omega_{pe}$ and $\Delta z > \lambda_{De}$). In each simulation, the normalized displacement that a thermal electron experiences per time step ($v_{te0}\,\Delta t/\Delta z \equiv [\omega_{pe}\,\Delta t]/[\Delta z/\lambda_{De}]$) was maintained at $\frac{1}{3}$ for all runs, where $v_{te0} \equiv \sqrt{T_{e0}/m_e}$ is the source electron thermal velocity. This was done such that the majority of the particles move less than one grid cell per time step, in order to avoid the associated finite-grid heating and cooling effects [15]. The time step, grid spacing, and particle injection rate per time step were all increased by a facor of 2 for successive simulations of the same physical system.

The distributed source model has a length $L = 128\lambda_{De0}$ with a mass ratio of $m_i/m_e = 100$, and a temperature ratio $T_{e0}/T_{i0} = 1$. The number of simulation particles at equilibrium was chosen to be $N_{e,i} \simeq 30{,}000$, such that the number of electrons per Debye length $N_D = (N_e\lambda_{De0}/L) \simeq 234$. Particle densities of this magnitude are required to obtain a constant potential profile in the source-free region [3]. For the given system configuration (system length, density, mass ratio, and temperature ratio), the time step Δt and grid spacing Δz were varied in five simulations from explicit to moderately implicit values: $\frac{1}{12} \leqslant \omega_{pe}\,\Delta t \leqslant \frac{4}{3}$ and $\frac{1}{4} \leqslant \Delta z/\lambda_{De} \leqslant 4$, with $32 \leqslant N_g \leqslant 512$ grid cells.

Figure 2a shows the variation of the steady-state, normalized potential drops $e\,\Delta\phi/kT_{e0}$ in the distributed source model as a function of the normalized grid spacing $\Delta z/\lambda_{De}$ and time step $\omega_{pe}\,\Delta t$. The numerical nature of the simulation changes from explicit to moderately implicit moving to the right in the figure. The source region, collector sheath, and total potential drops are represented as squares, circles, and triangles, respectively. The data points located at $\Delta z/\lambda_{De} = \omega_{pe}\,\Delta t = 0$ are predictions of the analytic model of Bissell and Johnson [2]. This steady-state, quasi-neutral model solves for the presheath potential profile and collector sheath drop, under the assumption that the electron density obeys a Boltzmann relation $n_e(z) = n_{e0}\exp(-e\phi/kT_{e0})$. All other data points are obtained from the fully kinetic particle simulations. The source region-potential drop $\Delta\phi_1$ is found to be insensitive to the size of the grid spacing (time step). This result is not unexpected, since the source region potential drop forms over the width of the distributed source region $L_S \simeq 51\lambda_{De}$. This behavior will continue as long as several grid cells are used to span the source region ($13 \leqslant L_S/\Delta z \leqslant 204$ in these simulations). The collector sheath drop $\Delta\phi_c$, which forms over the region of $\sim 5\lambda_{De}$ adjacent to the wall, is found to decrease as the size of the grid cell (time step) increases. The values of $\Delta\phi_c$ obtained from the theory and the simulations are in reasonable agreement (within 8.8%) for $\Delta z/\lambda_{De} \lesssim 1$. $\Delta\phi_1$ is measured between $z=0$ and $z=12.5$ cm ($\sim 7.7\lambda_{De}$), and $\Delta\phi_c$ is measured between $z=12.5$ cm and $z=L$.

The collector sheath drop is reduced by 62.6% from the theoretical values of Bissell and Johnson for the $\Delta z/\lambda_{De} = 4$ simulation. This produces a 44.7% reduction in the total potential drop ϕ_w from the theoretical value.

The planar source model also uses a system length $L = 128\lambda_{De0}$, with a temperature ratio $T_{e0}/T_{i0} = 1$, but the mass ratio for these simulations is $m_i/m_e = 50$. The injected electron flux was set to three and one-half times the injected ion flux: $\Gamma_{e0} = 3.5\Gamma_{i0}$. Once again, the number of simulation

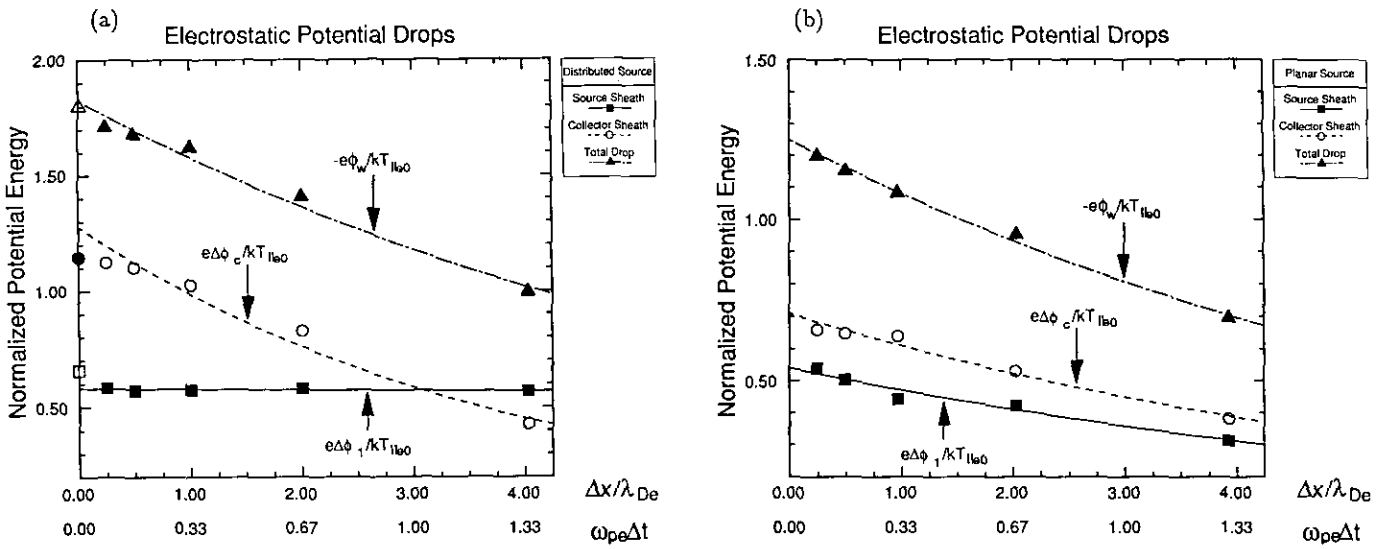

FIG. 2. Variation of source region potential drop, collector sheath, and total potential drops as a function of grid cell size Δz and corresponding Δt: (a) the distributed source model, and (b) the planar source model. The data points shown at $\Delta z/\lambda_{De}=0$ in Fig. 2a are obtained analytically [7]. The mass ratio is $m_i/m_e=100$ and the source temperature ratio is $T_{e0}/T_{i0}=1$.

particles at equilibrium ($N_{e,i}\simeq 31{,}000$) was fairly large, so as to maintain a particle density per Debye length ($N_D\simeq 256$) that was sufficient to obtain a flat potential profile outside of the source- and collector-sheath regions. Five simulations were performed with Δt and Δz in the range $\frac{1}{10}\leqslant\omega_{pe}\Delta t\leqslant\frac{4}{3}$ and $\frac{1}{4}\leqslant\Delta z/\lambda_{De}\leqslant 4$ (using $32\leqslant N_g\leqslant 512$ grid cells).

The dependence of the electrostatic potential structure in the planar source model on the size of the numerical parameters Δz and Δt is illustrated in Fig. 2b, where the simulations are explicit on the left and moderately implicit on the right. As before, the source region potential drop, collector sheath, and total potential drops are given by the square, circular, and triangular markers, respectively. In the planar source model, the source region potential drop forms over the region $\sim 5\lambda_{De}$ to the right of the emissive wall, which is the distance required to equilibrate the electron and ion fluxes that are injected at $z=0$. Therefore, both the source and collector sheaths in this system form on λ_{De} scale lengths. Both of these sheaths drops are found to decrease as the size of Δz and Δt are increased, each exhibiting a 42.1% reduction between the most explicit simulation ($\omega_{pe}\Delta t=0.10$, $\Delta z/\lambda_{De}=0.25$, and $N_g=512$ grid cells) and the most implicit simulation ($\omega_{pe}\Delta t=1.33$, $\Delta z/\lambda_{De}=3.93$, and $N_g=32$ grid cells). Once again, note that there is only a slight decrease in the collector sheath potential drop $\Delta\phi_c$ as the grid spacing is increased in the range $0.25\lambda_{De}\leqslant\Delta z\lesssim\lambda_{De}$.

The conclusion that can be drawn from the results presented in Fig. 2 is that sheaths which form on λ_{De} scale lengths are sensitive to the size of the time step and grid spacing used indirect-implicit particle simulations, but potential structures that form on scale lengths which encompass many grid cells are insensitive to the size of these numerical parameters. While the reduction of λ_{De} scale-length sheaths with increasing values of Δz and Δt may not be a surprising result, it is not clear whether this observation is due to the loss of spatial resolution of the electron Debye length, the loss of temporal resolution of the electron plasma period, or to some other cause. For instance, increasing the time step above the electron plasma period leads to damping of the high-frequency electrostatic modes, with a concurrent velocity drag on the particles (see Sections 2 and 5 of [11] for a complete description of these phenomena). This unphysical acceleration of the particles reduces their temperature (kinetic energy). The temperature of the electrons at the entrance to the collector sheath region, along with the ion to electron mass ratio m_i/m_e, determines the magnitude of the collector sheath potential drop [1, 2]. Therefore, the observed reduction of the λ_{De} scale-length potential drops may be due to finite grid-spacing *or* finite time-step effects, or to some other cause.

Since the simulations discussed above used the D_1 direct-implicit scheme [11], which produces a significant level of high-frequency mode damping, it is possible that the observed behavior is the result of finite time-step (damping) effects. To determine if this is the case, additional simulations of the distributed source model were performed with $\omega_{pe}\Delta t=\frac{4}{3}$ and $\Delta z/\lambda_{De}=4$, in which the level of damping was reduced towards zero. For the case of zero damping, the resulting algorithm is fully reversible and time-centered [13]. By decreasing the amount of damping from a high level (the D_1 scheme) to zero, numerical cooling of the plasma was reduced by 60.1%. In spite of this, both the

source region potential drop and collector sheath potential drops were found to be rather insensitive to the level of damping: $e\Delta\phi_1/kT_{e0} = 0.581 \pm 0.09$ for the D_1 scheme and 0.568 ± 0.08 for the fully reversible scheme, while $e\Delta\phi_w/kT_{e0} = 1.006 \pm 0.13$ for the D_1 scheme and 1.026 ± 0.25 for the fully reversible scheme.

Based upon these results, one may conclude that the reduction of λ_{De} scale-length sheaths does not arise from the loss of fine-scale temporal resolution incurred by using large time steps in implicit particle simulations. On the other hand, when the size of the grid spacing is increased above the Debye length, the number of grid cells that span the collector sheath region is significantly reduced. For the simulation in which $\Delta z/\lambda_{De} = 4$, the collector sheath region extends over only one to two grid cells. This resolution is too coarse to produce the correct potential profile in this large-electric-field region. Therefore, it seems likely that the loss of fine-scale spatial resolution that is associated with the use of large grid spacings is the root cause for the observed behavior. It is the poor spatial (and temporal) resolution of the collector sheath region in large Δz (Δt) implicit simulations that has motivated the development of the logical sheath boundary condition.

4. THE LOGICAL SHEATH BOUNDARY CONDITION

In this section the logical sheath boundary condition is formulated for use in the plasma-sheath models discussed in Section 2. We discuss more general applications of this boundary condition in Section 6. The collector sheath which forms adjacent to a floating wall has two effects. First, the negative potential drop (and corresponding electric field which is directed towards the wall) reflects most of the electrons, confining all but the most energetic ones. Second, the electric field accelerates the ions into the wall. For a floating wall, the collector sheath potential drop adjusts itself so that the electron and ion fluxes incident upon the wall are equal at steady state; that is, the net particle current to the wall is zero. Initially there is a transient stage of sheath formation in which the absorbing wall charges negative. At steady state the collector sheath prevents further accumulation of charge on the wall, such that the wall maintains a net negative charge. There are small fluctuations in the particle current at equilibrium, which are accounted for by the displacement current ($\sim\omega_{pe}$ type frequencies), such that the total current (displacement plus particle current) is zero.

If we assume steady-state conditions, then the continuity of charge may be expressed in integral form as

$$\oint_S \mathbf{J} \cdot d\mathbf{S} = 0, \tag{1}$$

where $\mathbf{J}$ is the total current density and S is an arbitrary closed surface. Taking S to be a surface around the conducting wall, Eq. (1) reduces to $I_{tot} = I_{ext}$, where I_{tot} is the total current into the wall from the plasma and I_{ext} is the current from the wall to an external circuit. For a floating wall $I_{ext} = 0$, so that the total current to the wall is zero ($I_{tot} = 0$). Rather than resolve all the details of the sheath region accurately, which requires the use of small time steps and grid spaces, we impose the equilibrium sheath physics at the wall in order to produce the "correct" sheath drop and electron velocity distribution. In the proposed model, the true spatial profile of the collector sheath potential is replaced by a negative step jump. Note that this is the correct analytic approximation in the limit $\lambda_{De} \to 0$. The location of the plasma-sheath interface is therefore $z = L$. The overall effect is to have no net charge and no electric field at the right boundary, which is quite different from the complete sheath description which has a wall charge and an electric field.

The algorithm for the logical sheath boundary condition is as follows:

I. Advance the trajectories of all electrons and ions.

II. Count the number of ions N_i and the number of electrons N_e which cross the wall boundary location each time step.

III. Compare N_e to N_i:

Case A. If $N_e \geqslant N_i$ (most probable condition) then:

1. Order the N_e electrons by velocity from fastest to slowest.

2. Absorb all N_i ions and the fastest N_i electrons.

3. Reflect the slowest $N_e - N_i$ electrons.

Case B. If $N_e < N_i$ then:

1. Absorb all N_i ions and N_e electrons.

2. Maintain a net *positive* wall charge σ_w for the following time step.

Since the electrons are the more mobile species, Case A ($N_e \geqslant N_i$) is the most probable condition. However, due to statistical fluctuations in the number of particles that hit the wall each time step, Case B ($N_e < N_i$) occasionally occurs. Case B ensures conservation of the total amount of charge in the system when $N_i > N_e$. The results using the logical sheath boundary condition (discussed below in Section 5) shows that Case B occurs approximately 7.0% of the time for the $\omega_{pe}\Delta t = \frac{1}{12}$ simulation, but this decreases to about 0.5% for the $\omega_{pe}\Delta t = \frac{2}{3}$ logical sheath simulation. Note that the wall charge σ_w is either zero (in Case A) or positive (in Case B). If $\sigma_w > 0$, this contribution to the total charge is included in the determination of the plasma potential ϕ. A schematic representation of the algorithm for Case A is shown in Fig. 3.

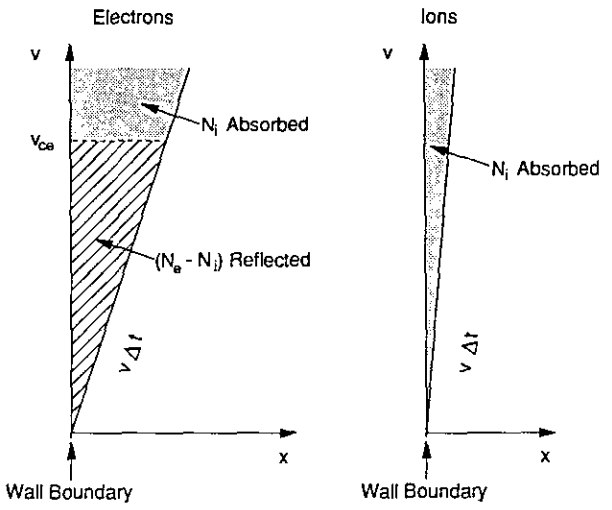

FIG. 3. A schematic representation of the logical sheath boundary condition. All the ions (N_i) and the fastest N_i electrons are removed from the system. The slower $N_e - N_i$ electrons are reflected.

The sheath drop is calculated from the electron cutoff velocity v_{ce}, which is taken to be the velocity of the slowest absorbed electron. The collector sheath drop is then calculated using conservation of energy via

$$\Delta\phi_c = \frac{m}{2e} v_{ce}^2, \tag{2}$$

where we have assumed that ϕ is not time varying. The potential drop $\Delta\phi$ is a result of the boundary condition and is only calculated for diagnostic purposes in the results presented in Section 5. For other applications, the potential drop may be needed to determine the wall physics, such as secondary electron emission, sputtering, or recycling.

For implementation of the logical sheath boundary condition into direct-implicit codes, it is necessary to use the algorithm for the advance to the intermediate location $\tilde{z}$ (the "pre-push"), as well as for the actual advance to the future time level (the "post-push") [6, 7, 10]. The reflection of excess electrons is required in the pre-push to calculate their contribution to the charge density $\tilde{\rho}$ and implicit susceptibility χ on the grid. Our implementation of the algorithm uses a simple shell sorting routine [16] to order the electron velocities.

The symmetry plane was introduced in our model to reduce the system size and number of particles by a factor of two. One could use the logical sheath boundary condition without a symmetry plane. The logical sheath boundary condition was first tested using the bounded explicit code PDW1 [17] at the collector sheath end without any symmetry condition imposed.

5. SIMULATION RESULTS WITH THE LOGICAL SHEATH BOUNDARY CONDITION

The logical sheath boundary condition algorithm has been tested within the framework of the bounded explicit code PDW1 [17] and the bounded direct-implicit code DIPSI [12]. In this section, results using the logical sheath boundary condition, as implemented in DIPSI, are compared with those using the conventional direct-implicit boundary conditions that are applicable to bounded plasma systems [14]. Two simulations of the distributed-source plasma-sheath model were performed with each boundary condition: a run with $\omega_{pe}\Delta t = \frac{1}{12}$ and $\Delta z/\lambda_{De} = \frac{1}{4}$ (which we will call the "small $\omega_{pe}\Delta t$" run) and a run with with an eight-times larger time step and grid cell size $\omega_{pe}\Delta t = \frac{2}{3}$ and $\Delta z/\lambda_{De} = 2$ (which we will call the "moderate $\omega_{pe}\Delta t$" run). The choice of these numerical parameters were made for the following reasons. First, we kept $v_{te}\Delta t/\Delta z = \frac{1}{3}$ in order to obtain an optimum level of energy conservation [15]. Second, we kept $\Delta z/\lambda_{De}$ small enough to ensure accurate resolution of the source region. The physical parameters were the same for all four runs. The mass ratio was $m_i/m_e = 100$ and the temperature ratio was $T_{e0}/T_{i0} = 1$. The total system length was $L \simeq 64\lambda_{De}$, where λ_{De} is calculated using the average, steady-state value of the electron density. The source length L_s was half the total system length. The time history plots are normalized by the thermal-ion transit time v_{ti0}/L, where $v_{ti0} = \sqrt{T_{i0}/m_i}$. Systems of this type typically equilibrate within a few thermal-ion transit times.

Figures 4 and 5 show the equilibrium electrostatic poten-

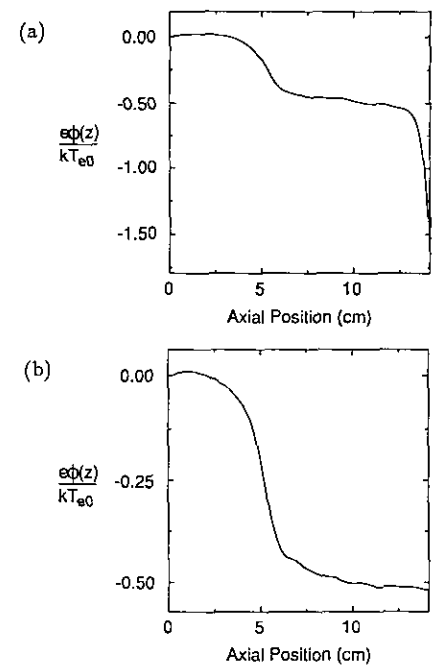

FIG. 4. Potential profiles obtained from the small $\omega_{pe}\Delta t$ runs with: (a) the conventional boundary condition; (b) the logical sheath boundary condition.

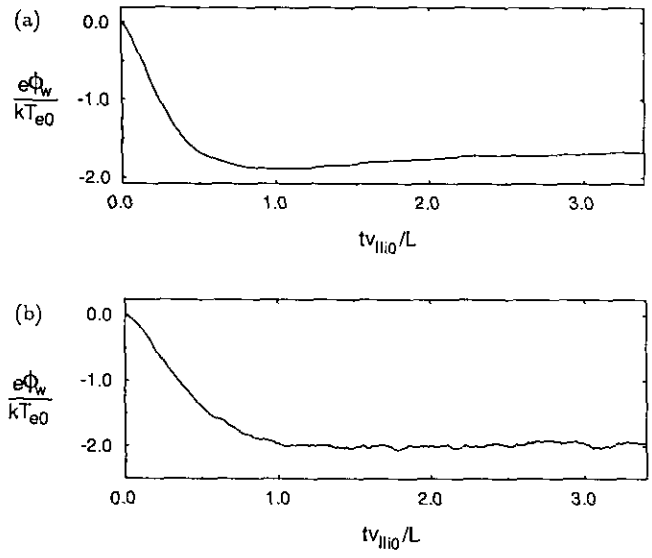

FIG. 5. Lag-averaged time histories of the total potential drop obtained from the small $\omega_{pe}\,\Delta t$ runs with: (a) the conventional boundary condition; (b) the logical sheath boundary condition.

tial profile and the lag-averaged time history of the total potential drop for the small $\omega_{pe}\,\Delta t$ run with the conventional and the logical sheath boundary conditions. Note that the collector sheath potential drop is *not* shown in Fig. 4b (and Fig. 6b to be described later). The results presented in Fig. 4a and 5a compare well with the predictions of the steady-state analytic theory of Bissell and Johnson [2], even though their model assumes that the electrons are governed by a Boltzmann factor and the particle code employs fully kinetic electrons (roughly a cutoff Maxwellian). The values of the source region potential drop, collector sheath, and total potential drops predicted by this theory, and those calculated by the particle simulations are presented in Table I.

The total potential drop calculated by the conventional, small $\omega_{pe}\,\Delta t$ simulation (shown in Fig. 4a and 5a), is within 6.3% of the analytic prediction. The quasineutral source sheath drop calculated by the small $\omega_{pe}\,\Delta t$ logical sheath run agrees well with that determined by the conventional, small $\omega_{pe}\,\Delta t$ run (see Figs. 4a and 4b). However, the collector sheath drop calculated in the logical sheath run is much larger than that calculated by the conventional, small $\omega_{pe}\,\Delta t$ model (23.7% larger; see Figs. 5a and 5b). This may be due to the large fluctuations in the electron cutoff velocity, and hence the collector sheath drop, arising from the small number of electrons and ions (N_e and N_i) that strike the wall per time step in the small $\omega_{pe}\,\Delta t$ simulation. For instance, these values are $\langle N_e\rangle = 4.7$ and $\langle N_i\rangle = 1.5$ for the small $\omega_{pe}\,\Delta t$ logical sheath run, and $\langle N_e\rangle = 36.2$ and $\langle N_i\rangle = 12.2$ for the moderate $\omega_{pe}\,\Delta t$ logical sheath run. The cutoff velocity is dependent upon the ratio $(N_e - N_i)/N_e$ (see Fig. 3), which is sensitive to the fluctuations in N_e and N_i. This ratio tends to increase with decreasing time step, leading to a larger average cutoff velocity and collector sheath drop. The small $\omega_{pe}\,\Delta t$ logical sheath run produces an average value of $\langle (N_e - N_i)/N_e\rangle = 0.744$, which decreases to $\langle (N_e - N_i)/N_e\rangle = 0.669$ for the moderate $\omega_{pe}\,\Delta t$ logical sheath run. It is expected that these fluctuations will decrease with increasing values of $nv_t\,\Delta t$, since this will increase the number of particles which cross the right boundary per time step, hence reducing the variance in this quantity.

In an effort to determine whether the small number of particles exiting per time step is the cause of the rather large collector drop, the small $\omega_{pe}\,\Delta t$ logical sheath run was repeated with approximately twice the number of particles (increasing the number of electrons from roughly 16,000 to 30,000). The results from this run are: $\langle N_e\rangle = 8.4$ and $\langle N_i\rangle = 2.8$, so that $\langle (N_e - N_i)/N_e\rangle = 0.698$. The average electron cutoff velocity was reduced from $\langle v_{ce}\rangle = 0.836 v_{te}$ to $\langle v_{ce}\rangle = 0.813 v_{te}$, where v_{te} is the electron thermal speed. The collector sheath drop was also reduced from $e\,\Delta\phi_c/kT_{e0} = 1.414 \pm 0.63$ to $e\,\Delta\phi_c/kT_{e0} = 1.254 \pm 0.40$ (which is only 9.7% larger than the analytic prediction). It is apparent that by increasing the values of N_e and N_i, the level of potential fluctuations and the mean value of the collector sheath drop are reduced, as is the mean value of the reflected electron fraction. Therefore, the accuracy with which the logical sheath model predicts the collector sheath drop *does* increase with an increase in the number of particles crossing the right boundary per time step. The source region potential drop and total potential drops from this run were $e\,\Delta\phi_1/kT_{e0} = 0.610 \pm 0.04$ and $-e\phi_w/kT_{e0} = 1.872 \pm 0.40$.

The fact that the discrepancy in the collector sheath drops obtained from the logical sheath simulations and the analytic theory decreases with increasing numbers of simulation particles suggests the following possible explanation. With fewer particles (i.e., poor counting statistics), the tail of the electron velocity distribution $f_e(v)$ is not well resolved and exhibits spikes, since the simulation particles are equally weighted as a function of velocity. The

TABLE I

Source Region Potential Drop ($\Delta\phi_1$), Collector Sheath ($\Delta\phi_c$), and Total Potential (ϕ_w) Drops Predicted Analytically and by Particle Simulations for $m_i/m_e = 100$ and $T_{e0}/T_{i0} = 1$

Source of results:	$e\,\Delta\phi_1/kT_{e0}$	$e\,\Delta\phi_c/kT_{e0}$	$-e\phi_w/kT_{e0}$
Analytic theory	0.655	1.143	1.798
Small $\omega_{pe}\,\Delta t$, conventional	0.542 ± 0.05	1.143 ± 0.13	1.685 ± 0.12
Small $\omega_{pe}\,\Delta t$, logical sheath	0.543 ± 0.04	1.414 ± 0.63	1.957 ± 0.63
Moderate $\omega_{pe}\,\Delta t$, conventional	0.558 ± 0.04	0.896 ± 0.10	1.454 ± 0.09
Moderate $\omega_{pe}\,\Delta t$, logical sheath	0.578 ± 0.04	1.142 ± 0.36	1.720 ± 0.36

simulation data seems to indicate that, as the statistics degrade with decreasing numbers of particles, the spikes in the electron velocity tail give the appearance of a higher effective electron tail temperature. There are only a few energetic electrons which make up these spikes in $f_e(v)$, but they force the collector sheath drop to be abnormally large in order to confine the required number of electrons as required for quasineutrality.

The equilibrium electrostatic potential profile and the lag-averaged history of the total potential drop for the moderate $\omega_{pe}\,\Delta t$ simulations, with the conventional and the logical sheath boundary conditions, are shown in Figs. 6 and 7, respectively. Comparing the potential profiles in Figs. 4a and 6a, we note that the moderate $\omega_{pe}\,\Delta t$ simulation produces an inaccurate prediction of the collector sheath drop, due to reduced resolution of λ_{De} scale length phenomena, but accurately reproduces the potential variation through the source and source-free regions. The collector sheath drop calculated by the conventional, moderate $\omega_{pe}\,\Delta t$ simulation differs from the analytic prediction of Bissell and Johnson by 21.6%. This error will increase with increasing Δt and Δz, as shown in Fig. 2a. The implicit simulation of the source region is still accurate, since this region has a much more gradual spatial variation which requires only moderate resolution in both time and space.

The source region potential drop calculated by the moderate $\omega_{pe}\,\Delta t$ logical sheath run agrees well with that

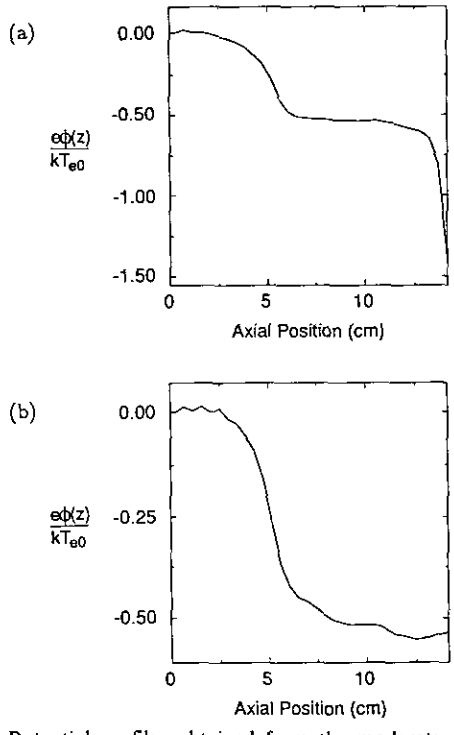

FIG. 6. Potential profiles obtained from the moderate $\omega_{pe}\,\Delta t$ runs with: (a) the conventional boundary condition; (b) the logical sheath boundary condition.

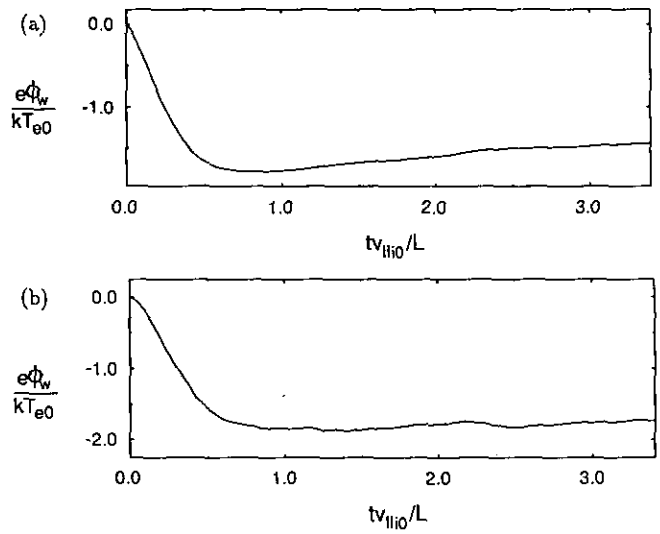

FIG. 7. Lag-averaged time histories of the total potential drop obtained from the moderate $\omega_{pe}\,\Delta t$ runs with: (a) the conventional boundary condition; (b) the logical sheath boundary condition.

determined by the conventional, small $\omega_{pe}\,\Delta t$ run. The collector sheath drop predicted by the moderate $\omega_{pe}\,\Delta t$ logical sheath run is in very good agreement with the predictions of both the analytic theory and the conventional, small $\omega_{pe}\,\Delta t$ run (0.1% difference). Increasing the time step (and grid spacing) by a factor of eight from small to moderate $\omega_{pe}\,\Delta t$, when using the logical sheath boundary condition, reduces the fluctuations in the collector sheath and total potential drops by 75% and substantially improves the accuracy of the calculated value of the collector sheath drop. These improvements are directly attributable to an increase in the number of particles crossing the wall per time step.

The time histories of the wall potential for all the runs (Fig. 5 and 7) show ϕ_w initially dropping in time and then reaching an equilibrium. For the conventional simulations the wall charges up negative during the transient then stays negatively charged. However, this is not the case in the logical sheath runs since no charge is accumulated at the right wall. It is interesting to note that the general time-dependent behavior is retained by the logical sheath model, even though the boundary condition is based on equilibrium physics.

6. DISCUSSION

A suitable boundary condition for the interface between the bulk plasma and an absorbing, conducting wall has been described which enables long time- and space-scale implicit simulations of bounded plasmas *without* having to resolve the short time- and space-scale collector sheath physics. The results from a particle simulation with moderate values of $\omega_{pe}\,\Delta t$ which uses the logical sheath boundary condition have been shown to compare well with

results from small $\omega_{pe}\Delta t$ simulations which resolve the sheath and with the predictions from analytic theory. We have been successful running implicit simulations with the particle code DIPSI using the logical sheath boundary condition with relatively large values of $\omega_{pe}\Delta t$ and $\Delta z/\lambda_{De}$ (with $\omega_{pe}\Delta t \gtrsim 10$ and $\Delta z/\lambda_{De} \gtrsim 31$) [18]. The accuracy of the logical sheath boundary condition does not depend on the resolution of ω_{pe} and λ_{De}, but rather improves by increasing the number of particles that cross the right boundary per time step ($nv_t\Delta t$).

Although the algorithm for the logical sheath boundary condition presented in Section 4 was specific to the one-dimensional plasma-sheath models of Section 2 (which do not allow for a magnetic field that is oblique or parallel to the wall), we do not envision any obstacles to implementation of the logical sheath in particle codes of higher dimensions or those with oblique magnetic fields. In a cross-field sheath, in which the applied magnetic field is parallel to the wall, the potential rises as one approaches the wall, since the electrons are strongly magnetized and well confined relative to the ions. We propose the following general algorithm for such cases: Advance the particle trajectories and count the number of electrons and ions that strike the boundary (N_e and N_i). If $N_e \geqslant N_i$ then proceed as in Section 4, Case A. However, if $N_i > N_e$, then sort the ions by velocity in descending order, and absorb all of the electrons and the fastest N_e ions. Then reflect the slowest $N_i - N_e$ ions. For two- or three-dimensional simulations the same algorithm could be used if one assumes that the boundary is a perfect conductor, since the entire boundary is fixed at the same potential in such a system.

Previous bounded particle simulation models [5] have included a more general external-circuit boundary condition than the floating wall considered to this point. In the proposed model, the net current to the wall (electrons plus ions) is specified to be zero. Alternatively, one could absorb or reflect particles to maintain a specified net current I_{ext}, which could be time-dependent. The net current I_{ext} would, of course, be limited by the right-going ion and electron fluxes at the wall: $-e\Gamma_e^+ < I_{ext} < e\Gamma_i^+$. Otherwise, it would be necessary to accumulate wall charge, and therefore, resolve the collector sheath. These additional logical sheath boundary conditions have not yet been tested.

ACKNOWLEDGMENTS

This work was performed at the University of California at Berkeley under U.S. Department of Energy Contract DE-FG03-86ER53220 and U.S. Office of Naval Research Contract N00014-85-K-0809. Support for R. J. Procassini was provided by the Plasma Physics Research Institute at the Lawrence Livermore National Laboratory, while B. I. Cohen was supported by the U.S. Department of Energy under Contract W-7405-ENG-48.

REFERENCES

1. G. A. Emmert, R. M. Wieland, A. T. Mense, and J. N. Davidson, *Phys. Fluids* **23**, 803 (1980).
2. R. C. Bissell and P. C. Johnson, *Phys. Fluids* **30**, 779 (1987).
3. L. A. Schwager and C. K. Birdsall, *Phys. Fluids B* **2**, 1057 (1990).
4. R. J. Procassini, C. K. Birdsall, and E. C. Morse, *Phys. Fluids B* **2**, 3191 (1990).
5. W. S. Lawson, *J. Comput. Phys.* **80**, 253 (1989).
6. A. Friedman, A. B. Langdon, and B. I. Cohen, *Commun. Plasma Phys. Controlled Fusion* **6**, 225 (1981).
7. A. B. Langdon, B. I. Cohen, and A. Friedman, *J. Comput. Phys.* **51**, 107 (1983).
8. R. J. Mason, in *Multiple Time Scales*, edited by J. U. Brackbill and B. I. Cohen (Academic Press, New York, 1985), 233.
9. J. U. Brackbill and D. W. Forslund, in *Multiple Time Scales*, edited by J. U. Brackbill and B. I. Cohen (Academic Press, New York, 1985), 272.
10. A. B. Landon and D. C. Barnes, in *Multiple Time Scales*, edited by J. U. Brackbill and B. I. Cohen (Academic Press, New York, 1985), 336.
11. B. I. Cohen, A. B. Langdon, and A. Friedman, *J. Comput. Phys.* **46**, 15 (1982).
12. R. J. Procassini and B. I. Cohen, Report UCRL-ID 104093, Lawrence Livermore National Laboratory, Livermore, 1990 (unpublished).
13. A. Friedman, *J. Comput. Phys.* **90**, 292 (1990).
14. S. E. Parker, C. B. Birdsall, A. Friedman, and S. L. Ray, *Bull. Am. Phys. Soc.* **32**, 1855 (1987); Paper 6S7.
15. B. I. Cohen, A. B. Langdon, D. W. Hewett, and R. J. Procassini, *J. Comput. Phys.* **81**, 151 (1989).
16. W. H. Press, B. P. Flannery, S. A. Teukolsky, and W. T. Vetterling, *Numerical Recipes* (Cambridge Univ. Press, New York, 1986), p. 228.
17. W. S. Lawson, Report UCB/ERL M84/37, Electronics Research Laboratory, University of California, Berkeley, 1984 (unpublished).
18. R. J. Procassini, C. K. Birdsall, and B. I. Cohen, *Nucl. Fusion* **30**, 2329 (1990).